THE JOURNAL OF PHYSICAL CHEMISTRY B
A JOURNAL OF THE AMERICAN CHEMICAL SOCIETY

pubs.acs.org/JPCB

Article

Programmable Crowding and Tunable Phases in a Binary Mixture of Colloidal Particles under Light-Driven Thermal Convection

Jose Lopez-Ceja, Vanessa Flores, Shirlaine Juliano, Sean Machler, Stephen Smith, Gargi Mansingh, Meng Shen, and Nabila Tanjeem*

Cite This: J. Phys. Chem. B 2024, 128, 9244−9254

Read Online

ACCESS | Metrics & More | Article Recommendations | Supporting Information

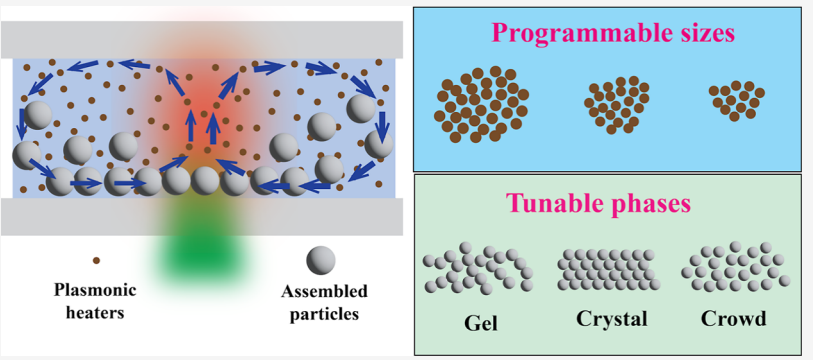

ABSTRACT: We employ photothermally driven self-assembly of colloidal particles to design microscopic structures with programmable size and tunable order. The experimental system is based on a binary mixture of "plasmonic heater" gold nanoparticles and "assembly building block" microparticles. Photothermal heating of the gold nanoparticles under visible light causes a natural convection flow that efficiently assembles the microscale building block particles (diameter 1−10 μm) into a monolayer. We identify the onset of active Brownian motion of colloidal particles under this convective flow by varying the conditions of light intensity, gold nanoparticle concentration, and sample height. We realize a crowded assembly of microparticles around the center of illumination and show that the size of the particle crowd can be programmed using patterned light illumination. In a binary mixture of gold nanoparticles and polystyrene microparticles, we demonstrate the formation of rapid and large-scale crystalline monolayers, covering an area of 0.88 mm^2 within 10 min. We find that the structural order of the assembly can be tuned by varying the surface charge of the nanoparticles and the size of the microparticles, giving rise to the formation of different phases—colloidal crystals, crowds, and gels. Using Monte Carlo simulations, we explain how the phases emerge from the interplay between hydrodynamic and electrostatic interactions, as well as the assembly kinetics. Our study demonstrates the promise of self-assembly with programmable shapes and structural order under nonequilibrium conditions using an accessible setup comprising only binary mixtures and LED light.

INTRODUCTION

The self-organization of microscopic colloidal particles driven by external stimuli is an intriguing field of study for its appeal to both fundamental research and application design. On the one hand, our understanding of nonequilibrium self-assembly that is ubiquitous in biology is enriched by laboratory experiments performed on active colloids and their collective behavior.[1−3] Active colloids consume energy from external stimuli to drive their motion, and interaction between many active colloids results in various forms of self-organized collective states. Living crystals,[4] phase separation,[5,6] pattern formation,[7−9] swarms and swirls,[10,11] and active transport[12,13] are some remarkable manifestations of these collective states. On the other hand, colloidal self-assembly induced by light, electric, and magnetic fields has emerged as a rapid and bottom-up technology for micro- and nanofabrication. Programmable and reconfigurable self-assembled structures can be designed by modulating an external field, as demonstrated in self-assembled microswimmers,[14,15] dissipative crystals,[16] shapeshifting clusters,[17−19] and tunable color applications.[20−22] Because of the variety of utilities, it is essential to understand and develop new methods that expand our understanding of out-of-equilibrium self-organization.

Received: April 8, 2024
Revised: June 21, 2024
Accepted: July 16, 2024
Published: July 24, 2024

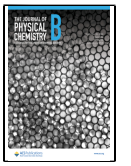

https://doi.org/10.1021/acs.jpcb.4c02301
J. Phys. Chem. B 2024, 128, 9244−9254

Light-driven systems are particularly promising for enabling spatiotemporal control over self-assembly dynamics.[23−25] Light-induced assemblies are widely investigated in experimental systems where a photochemical or photothermal response is designed into chemically synthesized colloidal particles[26−30] or surfactants.[16] The need for sophisticated material synthesis can be bypassed in systems based on photothermal effects—where a temperature gradient is generated in a particle suspension that drives the convective or thermophoretic movement of particles, resulting in their self-organization.[31] These systems have been used for optical trapping,[32−35] self-assembly,[36−40] patterning,[41] sorting,[42] and crystallization[43−46] of colloidal particles. Although high-power infrared lasers were used for heat generation in early studies, plasmonic substrates and nanoparticles have been employed recently for efficient self-assembly driven by visible light.[36,37] Despite these promising results, photothermal convection experiments have not yet been mainstream in the study of nonequilibrium colloidal self-assembly due to their limited scope in programmability.

We demonstrate a new experimental system that allows for rapid photothermal self-assembly of colloidal particles into structures with programmable size and tunable order. Our system can be implemented using commercially available gold nanoparticles and high-intensity LED light sources widely used for fluorescence microscopy, thereby eliminating the need for high-intensity lasers, expensive nanofabrication, or synthesis that were required in prior work. The system works based on a binary mixture of "plasmonic heater" particles and "assembly building block" particles; photothermal heating of the plasmonic heater gold nanoparticles (AuNP, diameter d = 15 nm) under visible light generates a temperature gradient, causing a convection flow that assembles the "building block" particles (diameter D = 1 μm−10 μm). The drag force causes the smaller heater particles to follow the convective flow while the larger particles sediment near the bottom of the sample chamber due to gravity and thermophoresis and form a self-assembled monolayer (Figure 1a). This system allows us to achieve two different forms of tunability—in the shape and in the structural order of self-assembly. A patterned light illumination setup is employed to define the landscape of the photothermal effects, allowing for the programming of the size of the assembled structure. By using a binary mixture of gold nanoparticles (heaters) and colloidal polystyrene (building blocks) particles, we can form large 2D polycrystals with an area as large as 0.88 mm^2 in less than 10 min using only 14.6 mW power from LED light. We find that the structural order of the assembly can be tuned by varying the electrostatic interactions and the size ratio of the two particles, resulting in the emergence of three different phases—hexagonally packed crystals, particle crowds (a dense but fluid state of assembly), and colloidal gels.

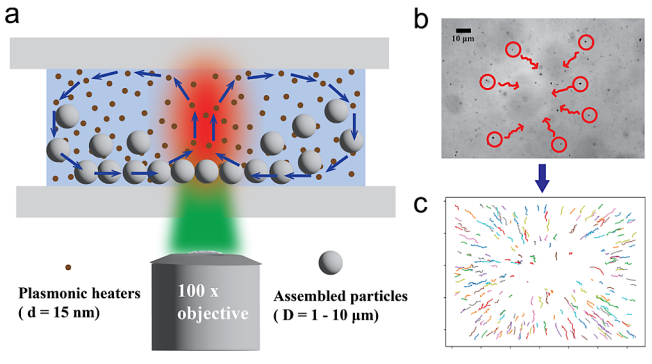

Figure 1. (a) Illustration of the experiment setup. Binary mixture of "heater" and "building block" particles is illuminated with LED light through the microscope objective. Convection flow (blue arrows) is generated from the photothermal response of the heater particles. Due to gravity and thermophoresis, the larger building block particles form a self-assembled monolayer near the bottom wall of the sample chamber. (b) Gold nanoparticle clusters identified from a microscope image. (c) Trajectories of the identified clusters under light illumination calculated from a series of microscope images.

METHODS

Preparation of Gold Nanoparticle Suspension. The gold nanoparticles used in the binary mixture self-assembly were purchased from Nanopartz Inc. (product #A11-15-CTAB-DIH-1-25, #A11-15-CIT-DIH-1-25). A total of 4 mL particle suspension was centrifuged (using Eppendorf 5430) at 12,000 rpm for 15 min and then was redispersed in 100 μL of Milli-Q water. The absorption spectrum of the gold nanoparticle suspension was measured using a UV−vis spectrometer (PASCO, SE-3607).

The gold nanoparticles used for the programmable crowd assembly were synthesized at the laboratory using a seed-mediated growth method.[47,48] The seed solution was prepared by mixing 100 mM Cetyltrimethylammonium Bromide (CTAB) with 50 mM gold(III) Chloride trihydrate ($HAuCl_3 \cdot 3H_2O$) and 10 mM sodium borohydride ($NaBH_4$). We prepared the 100 mM CTAB solution by dissolving 0.546 g of CTAB in 15 mL of Milli-Q water and then heated up the solution to 40 °C in an ultrasonic bath until it became transparent. The 50 mM gold salt was prepared by dissolving 59 mg of $HAuCl_3 \cdot 3H_2O$ with 3 mL of Milli-Q water. The 10 mM sodium borohydride solution was prepared by dissolving 11 mg of $NaBH_4$ into 30 mL of ice-cold Milli-Q water. A glass vial was filled with 5 mL of the 100 mM CTAB solution and set up with magnetic stirring at 950 rpm. Twenty-five μL of gold salt and 300 μL of $NaBH_4$ were added to the mixture while stirring. The solution turned brown immediately, confirming the formation of gold seeds. The solution was stirred for 5 min and then left at room temperature for at least an hour.

The gold seeds were then grown into gold nanoparticles by mixing with more gold salt, CTAB, and ascorbic acid. We diluted the 100 mM CTAB solution with Milli-Q water to prepare a 0.1 mM CTAB solution and put 5 mL of it in a glass vial. A 100 mM ascorbic acid solution was prepared by dissolving 35 mg of ascorbic acid into 2 mL of Milli-Q water. The 5 mL 100 mM CTAB solution was set up in a glass vial under magnetic stirring (300 rpm at 28 °C in an oil bath). Fifteen μL of the ascorbic acid solution, 20 μL of the 50 mM gold salt solution, and 30 μL of the gold seed solution were added in that order while stirring. The solution turned purple and then red within 15 min, indicating the successful synthesis of gold nanoparticles. The nanoparticles were then centrifuged in two steps (first at 7800 rpm in 50 mL tubes, then at 12,000 rpm in 1.5 mL tubes) and were dispersed in 100 μL of Milli-Q water.

Preparation of Binary Mixture Samples. To prepare a binary mixture, 5 μL of 15 nm gold nanoparticle solution was mixed with 5 μL of 1% w/v polystyrene (PS) particles. The PS particles used in this experiment (D = 1, 2, and 5 μm) were purchased from Thermo Fisher Scientific (catalog number C37274, C37278, and C37255) and were suspended in Milli-Q water. The 10 μL binary mixture suspension was mixed well with a micropipette before placing it in a sample chamber. The

https://doi.org/10.1021/acs.jpcb.4c02301
J. Phys. Chem. B 2024, 128, 9244−9254

sample chamber was prepared using two glass coverslips (VWR Micro Cover Glasses No. 1). A thin square-shaped frame of vacuum grease was placed onto the 50 × 22 mm coverslip before the 10 μL particle suspension was placed inside the frame. Afterward, another coverslip (22 × 22 mm) was placed on top of the sample and pressed until the vacuum grease layer seals the sample solution adequately from all sides. The thickness of the sample chamber was determined by the thickness of the vacuum grease layer and was measured to be about 360 μm. The prepared sample chamber was immediately taken to the microscope for light irradiation and imaging.

Imaging and Light Irradiation Setup. All experiments were performed using an inverted microscope (Olympus ix83) equipped with a high-speed CMOS camera (Moment, Teledyne Photometrics). All imaging was performed under bright-field conditions using a Halogen lamp. Two different light sources were used for photothermal convection experiments. The LED light source (X-Cite XYLIS from Excelitas technologies) with epi-illumination settings was used for the full-field illumination experiments. The light irradiation and image capture were performed using the open-source software Fiji and its plug-in Micromanager 2.0. For patterned light illumination, a digital micromirror device (DLPLCR95EVM and its controller board, DLPLCRC410EVM from Texas Instruments) was used along with a high-power LED light source purchased from Thorlabs (SOLIS-565C). The LED was set up at an angle such that the reflected light from the digital micromirror device (DMD) travels to the microscope's optical path through a lens (focal length 150 mm). The light pattern from the DMD was then projected onto the sample plane through the microscope objective (100×, NA = 1.45).

Particle Tracking and Image Analysis. An open-source Python package, "Trackpy" was used to identify gold nanoparticle clusters from microscope images and to track their motions from video frames. First, the gold nanoclusters were identified from images by using three different parameters—particle diameter, minimum separation distance between the identified particles, and minimum brightness of the features. The minimum separation distance was set to a value about four times larger than the particle diameter to avoid overlapping particle trajectories. Next, the positions of the particles were tracked over multiple images (up to 200 frames at a frame rate of 50 frames per second) using an adjustable parameter—the minimum distance traveled by a particle between two adjacent frames. To achieve greater accuracy in tracking, we ignored the particles that went out of focus before being observed for at least 15 frames consistently. We performed an additional inspection on the tracked particles and filtered out the trajectories of stationary particles that were attached to the glass coverslip. We applied an ensemble mean-squared displacement analysis on the particle trajectories to find the fitting parameter n from MSD = Ct^n. To calculate the mean hexatic order parameter and bond length from microscope images of colloidal crystals, we first identified the particle positions using Trackpy. Then, we developed a Python script to calculate the $\overline{\psi}_6$ and $\overline{D}_B$ parameters from the particle coordinates. We used Fiji to analyze particle crowds and measure crowd sizes from patterned light experiments. We set a threshold brightness to isolate the pixels that are darker (in less than 30−40th percentile) from the background and applied a tracing tool to identify the area of the dark region. An example of the measurement is presented in Figure S3. We found the uncertainty in determining the accurate threshold to be smaller than the error bars on the plot.

Calculation and Measurement of Solution Temperature. To estimate the temperature increase ΔT in a gold nanoparticle suspension, we defined a 3-dimensional cube (100 × 100 × 100 μm) and placed $N = 3.5 \times 10^7$ particles randomly in the cube using a home-built Python script. We calculated Q (generated heat by one nanoparticle) using the values of relevant known constants (SI Section 2) and our experimentally measured light intensity. Then we measured the temperature increase at a random point in the cube (e.g., the origin of the cube) using the equation $\Delta T = \sum_i \frac{V_{NP}Q}{4\pi k_0 r_i}$, where r_i is the distance from the ith nanoparticle position to the point where the temperature is calculated. We experimentally estimated the solution temperature by observing the melting temperature of 100 mM CTAB solution. 100 mM CTAB forms large solid phases at room temperature (20 °C) that can be observed under an optical microscope. When mixed with gold nanoparticles (5 μL CTAB and 5 μL AuNP), we observed the melting of the CTAB solid phase under the same conditions of light irradiation that was used for the photothermal convection experiments. We prepared another CTAB AuNP mixture sample and left it in an oven at different temperatures to identify its melting temperature in the absence of light illumination. We observed the CTAB phases under three different temperatures − 20, 25, and 30 °C and found that the solid structures melt after leaving at 30 °C, confirming that the melting temperature is in between 25 and 30 °C.

RESULTS AND DISCUSSION

Colloidal Particle Motion under Light-Driven Photothermal Convection. We characterized the motion of colloidal particles under photothermal convection flow generated by the plasmonic heater gold nanoparticles for different conditions of light intensity, gold nanoparticle concentration, and sample height. For this experiment, we illuminated a gold nanoparticle suspension (purchased from Nanopartz Inc., CTAB functionalized, the average diameter d = 15 nm) with an LED (X-Cite XYLIS, wavelength λ = 540−560 nm). An inverted optical microscope (Olympus ix83) equipped with a 100× oil immersion objective lens (NA = 1.45) was used to observe the particle dynamics in real-time. The surface plasmon resonance peak of the gold nanoparticles suspension was measured to be at λ = 520 nm (Figure S1), and 93% of the peak absorbance was measured at 540 nm − the excitation wavelength of the LED. An inward flow of particles toward the center of light irradiation was observed about 10−30 μm above the bottom wall of the sample chamber (Figure 1b). The threshold light intensity above which the flow occurred was about 135 W/cm^2 and the threshold initial concentration of the gold nanoparticles in the suspension was about 10^{13} particles/mL. Since the individual gold nanoparticles (d = 15 nm) are much smaller than the Abbe diffraction limit of the microscope, we measured the flow by tracking the motion of a few nanoparticle clusters found in the suspension (diameter in the range of 0.5−1 μm, marked with red circles in Figure 1b). These clusters form likely due to imperfection in the particle synthesis process or the sample preparation steps. The trajectories of the tracked particles (as shown in Figure 1c) resemble active Brownian motion—a directional motion toward the light accompanied by random fluctuations. We fit the mean-squared displacements (MSD) of the particle ensemble with the equation MSD = Ct^n, to find n for different experimental

https://doi.org/10.1021/acs.jpcb.4c02301
J. Phys. Chem. B 2024, 128, 9244−9254

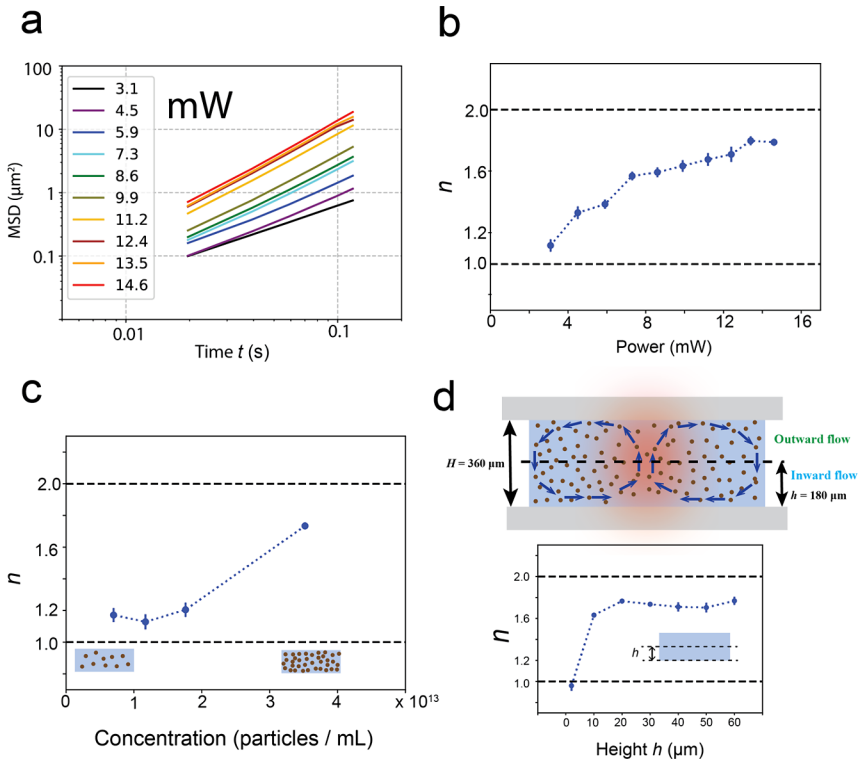

Figure 2. (a) Mean-squared displacement (MSD) over time plot in log−log scale for different light intensities, represented by the differently colored lines. Increasing slope of the lines with higher light power indicates increased active Brownian motion. (b) Plot showing the increase of n with light power; n is calculated from fitting the MSD = Ct^n equation using the data from (a). (c) Value of n increases with the nanoparticle concentration in the suspension. (d) Top: an illustration of the velocity field of the convection flow at different heights of the sample chamber, estimated from the direction of the flow observed near the top and the bottom walls of the chamber. Bottom: the value of n at different heights from the bottom wall of the sample chamber.

parameters such as light intensity, gold nanoparticle concentration, and sample height.

The active motion of the tracked particles increases with light power (as shown in Figure 2a,b), with the values of n in the range of 1.1−1.8. Each straight line on the plot of Figure 2a represents an ensemble average over the trajectories of 100−200 particles tracked and analyzed from videos recorded at the speed of 50 frames per second. While at low light intensity, the particle motion resembles purely Brownian motion ($n \cong 1$), they become highly active at about 14.6 mW of light power ($n \cong 2$ for ballistic motion). The value of n in the range of $1 < n < 2$ indicates that the particles exhibit a combination of Brownian motion and active motion due to photothermal convection. Under nearly ballistic conditions ($n \cong 2$), the fluid velocity derived from the MSD calculations is 30.3 μm/s. For all experiments performed at different light intensities, we set the initial particle concentration as 3.5×10^{13} particles/mL, and recorded particle trajectories at a constant height -30 μm above the bottom wall of the sample chamber.

To measure the onset of the photothermal convection, we characterized particle motion by varying the concentration of the nanoparticle suspension while illuminating 14.6 mW of light. As shown in Figure 2c, we find a significant increase in particle activity (n = 1.8) when the particle concentration was at 3.5×10^{13} particles/mL, in comparison with a sample with lower particle concentration ($n \cong 1.2$ at particle concentration $\leq 2 \times 10^{13}$ particles/mL). We estimate a temperature increase of ΔT = 9 °C at the illuminated region compared to its surroundings (room temperature about 20 °C) for a nanoparticle concentration of 3.5×10^{13} particles/mL. The velocity of photothermal convective flow increases linearly with the temperature difference between the heated sample and its surroundings, ΔT.[38,49] The flow velocity can be expressed as,

$$v = w^2 \rho g \beta \frac{\Delta T}{\eta} \tag{1}$$

where w: width of the light beam, ρ: fluid density, β: thermal expansion coefficient of the fluid, and η: dynamic viscosity.

The temperature increase ΔT can be calculated from the expression of total heat generation in a gold nanoparticle suspension:[50,51]

$$\Delta T = \sum_i \frac{V_{NP} Q}{4\pi k_0 r_i} \tag{2}$$

where V_{NP}: volume of one nanoparticle, k_0: thermal conductivity of water, and r_i: distance between the ith nanoparticle surface and the point of temperature measurement. Q is the heat generated by one gold nanoparticle and can be expressed by the following equation (see SI Section 2 for parameters used in the temperature estimation):

$$Q = \frac{\omega I}{c\sqrt{\varepsilon_0}} \left| \frac{3\varepsilon_0}{2\varepsilon_0 + \varepsilon_{NP}} \right|^2 \mathrm{Im}\left(\varepsilon_{NP}\right) \tag{3}$$

Additionally, we performed an experimental measurement of the temperature increase by melting crystals of cetyltrimethylammonium bromide (CTAB) − an amphiphilic molecule commonly used in gold nanorod synthesis. In a 100 mM CTAB aqueous solution, large solid structures form at room temper-

https://doi.org/10.1021/acs.jpcb.4c02301
J. Phys. Chem. B 2024, 128, 9244−9254

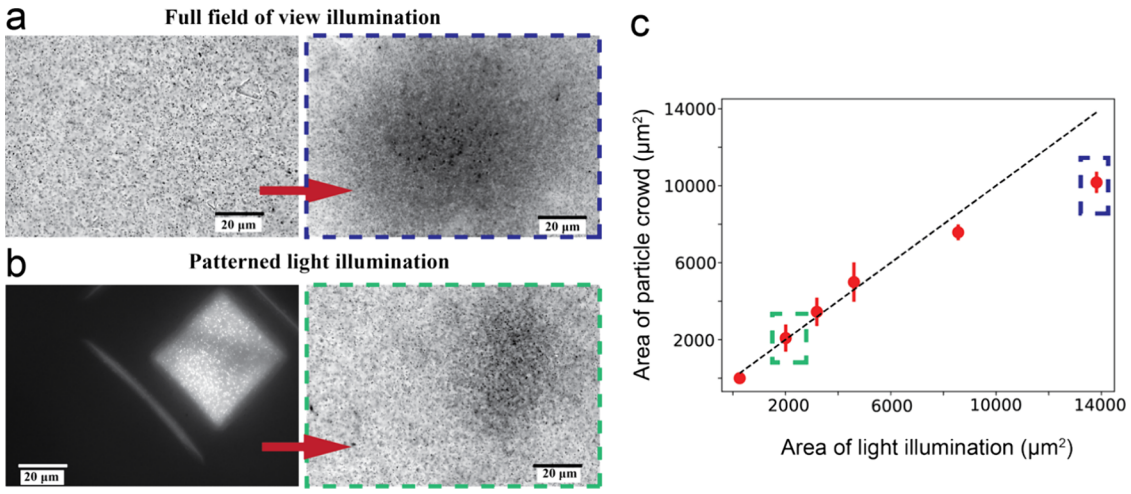

Figure 3. (a) Gold nanoclusters in an aqueous suspension form a crowded assembly under full-field light illumination (without DMD). Left: particles in a fluid state without any light illumination. Right: particles form a crowded (dense fluid) state after 15 min of flood illumination. (b) Same suspension forms a particle crowd with a size and shape defined by the square-shaped pattern. Left: the square-shaped light projected onto the sample using a DMD. Right: an image of the particle crowd formed after 15 min of patterned light illumination. (c) Area of the assembled crowd increases linearly with the area of illuminated region. Black dotted line represents the straight line for crowd area = illuminated area.

ature (20 °C) that can be melted at about 30 °C (SI Section 3). We observed light-driven melting of CTAB crystals (Figure S2) when mixed with a gold nanoparticle suspension of concentration 3.5×10^{13} particles/mL, confirming that the heightened temperature at the illuminated region is indeed close to 30 °C ($\Delta T \cong 9$ °C). Applying this measured temperature increase to eq 1, we calculate the velocity of the convection flow to be 50.8 μm/s − which is within the same order of magnitude as the fluid velocity (30.3 μm/s) measured from the trajectories shown in Figure 1c. The agreement between the experiment and calculation confirms that the major contributor of the particle flow is indeed photothermal convection generated by the gold nanoparticle suspension.

Lastly, we observed the flow and quantified the active Brownian motion of particles at different sample heights. The total thickness of our sample chamber was $H = 360$ μm; an inward flow was observed at heights $h \leq \frac{H}{2}$, while an outward flow was observed at heights $h > \frac{H}{2}$. To image through the entire depth of the chamber, we switched to a 10× objective and used large particles (10 μm) as tracers. This observation is consistent with the flow pattern of photothermal convection reported in prior work.[36,37] Furthermore, by quantifying particle activity at different heights at the sample chamber ($h = 2-60$ μm) as shown in Figure 2d, we recorded highly active Brownian motion ($n = 1.6$) at about $h = 10$ μm above the bottom wall of the sample chamber.

Programming the Size of Colloidal Assembly Using Patterned Light. Photothermal convection flow allows particles that are larger in size and denser than the fluid to accumulate near the center of the illuminated region.[36] We show that the shape of the assembly can be programmed by employing patterned light illumination. A digital micromirror device (DMD) was used to generate and project different light patterns onto the sample plane of the microscope. In this experiment, we used gold nanoparticles synthesized at the lab using the seed-mediated growth method[47] with an estimated average diameter of 50 nm (UV−vis spectra in Figure S1). Because of synthesis imperfection, a non-negligible number of particle clusters form (small dark spots on Figure 3a: left, diameter in the range of 0.5−1 μm). Photothermal convection flow generated by the 50 nm particles (not visible under the optical microscope) helps assemble the large clusters into a crowded state (large dark region in Figure 3a: right, and Movie S1). Under flood illumination without any projected pattern, a crowd of particles with a circular shape assemble around the center of the illumination (Figure 3a: right). The assembly of the particles forms in a dense fluid state that gets dispersed when the light is turned off; hence, we define this assembly as a "particle crowd."

We can program the position and the shape of the particle crowd assembly by using a much smaller illumination zone, as shown in Figure 3b (left). Under this patterned illumination, the position of the formed crowd matches the position of the square-shaped light pattern, and the crowd size is approximately equal to the size of the square with a side length of 45 μm. To identify the scope of the programmability, we applied square and rectangular-shaped light patterns with different areas and found that the area of the formed crowds increases with the area of the projected illumination patterns (Figure 3c). Although a previous study on photothermal convection-driven self-assembly has indicated that the size of the assembly is roughly equal to the width of a laser beam,[46] our study is the first to demonstrate that assembly size can indeed be varied and programmed using patterned light illumination.

Rapid and Large-Scale Photothermal Self-Assembly of Colloidal Crystals. Upon confirming that photothermal convection generated by gold nanoparticles (AuNP) successfully assembles larger microscale colloids, we use the AuNPs as "plasmonic heaters" to drive the self-assembly of "building block" colloidal particles that are uniform in size. Our strategy is to prepare a binary mixture of two different particle species: AuNPs with an average diameter of $d = 15$ nm and polystyrene (PS) particles with an average diameter in the range of $D = 1-10$ μm. Because of the 2−3 orders of magnitude difference in the sizes of the two particle species, we can successfully self-assemble the building block PS particles into a monolayer.

First, we demonstrate the assembly of PS particles with $D = 10$ μm using our binary system. Unlike the gold nanocluster suspension, the large PS particles form a self-assembled crystalline monolayer, as shown in Figure 4a,c. The diffusion

https://doi.org/10.1021/acs.jpcb.4c02301
J. Phys. Chem. B 2024, 128, 9244−9254

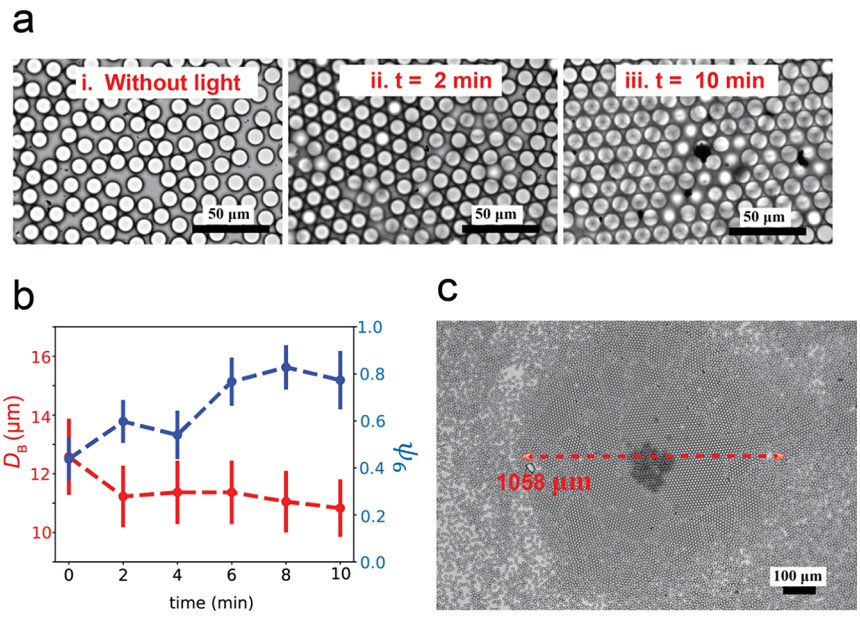

Figure 4. (a) Formation of a crystalline monolayer of PS colloidal particles (D = 10 μm) under light irradiation of 10 min. (b) Average hexatic order parameter (blue) and bond length (red) plotted over time, calculated from microscope images of the crystals presented in (a). (c) Total region of crystal formation viewed using a 10× objective.

constant of the 10 μm particles are very small (~0.05 $\mu m^2/s$), and they sediment close to the bottom wall of the sample chamber due to gravitational force. However, under light illumination of 10 min, the area fraction covered by the particles increased from 63% (Figure 4a,i) to 84.7% (Figure 4a,iii). In between 2 and 10 min, we observe two crystalline grains merged to form one large grain, indicating that coarsening takes place rapidly under the convection flow. The assembly of the PS particles remains mostly free of AuNPs; however, we observe occasional formation of gold nanoparticle clusters (a dark spot in Figure 4c near the center) that accumulate on top of the crystalline monolayer formed by the 10 μm PS particles.

The formation of the large crystalline region from photothermal effects can be attributed to a combined action of convection and thermophoresis. As presented in the computational model by Park et al.,[36] particles smaller than 100 nm flow along the streamlines of the convective flow due to drag force, while particles that are larger in size (>2 μm) or denser than the fluid (>1.2 g/cm^3) tend to form an assembled monolayer because of gravitational force. In our experiment, although particle density (polystyrene, 1.1 g/cm^3) is marginally smaller than 1.2 g/cm^3, the much larger particle size indicates that gravity likely helps maintain the separation between the large 10 μm PS particles and the small 15 nm gold AuNPs. However, prior work by Duhr and Braun[43] suggested that while convection allows for the accumulation of large and dense particles, it is not enough to assemble a closely packed crystalline monolayer. Weinert and Braun[52] have shown that thermophoretic slip flows appear near particle surfaces in the presence of a wall at a high temperature gradient ($S_T a \nabla T \gg 1$, a: particle radius, S_T: Soret coefficient). When interparticle distances are small, the flow fields of multiple particles overlap, giving rise to a long-ranged, hydrodynamic attractive interaction.[44] Nucleation of small crystallites in a dilute suspension (0.05% w/v) of D = 10 μm was observed in 90 s (Figure S4) that indicates the presence of an attractive pair potential between particles, resembling a long-ranged hydrodynamic interaction. Therefore, our observation of crystal formation is consistent with these previous studies and likely is a result of the combined actions of convection, thermophoresis, and gravity. The distinction from prior work is that we successfully demonstrate rapid crystallization with a much lower light power (14.6 mW) thanks to the efficient heat generation by the heater AuNPs.

We calculated the average hexatic order parameter, $\overline{\psi_6} = \frac{1}{n}\sum_{j=1}^{n} e^{6i\theta_j}$ and average bond length, $\overline{D}_B$ (center-to-center distance between neighboring particles) to quantify how crystallization progresses over time. Within 2 min of light illumination, small crystallites start forming (as shown in Figure 4a,ii), and after 10 min, average hexatic order $\overline{\psi_6}$ reaches its maximum value (0.8) and average bond length $\overline{D}_B$ reaches its minimum value (10.8 μm) (Figure 4b). Additionally, we find a wide circular region of polycrystal formed with an area of 0.88 mm^2 as shown in Figure 4c. This area is much larger compared to the crowd formation under full-field illumination on gold nanoclusters (0.01 mm^2, Figure 3a) indicating that the self-assembly under photothermal effects has a strong dependence on the size of the building block particles.

Formation of Different Colloidal Phases: Crystals, Crowds, and Gels. To investigate the extent of structural tunability, we examined binary mixtures with varying sizes of the building block particles and different electrostatic interactions between the building block and heater particles. First, we show that the electrostatic interactions play a major role in determining the self-assembled structure in a binary system with constant particle sizes. For this experiment, we prepared a binary mixture of building block PS particles with a diameter of D = 2 μm and gold nanoparticles (d = 15 nm). We kept the surface functionalization of the PS particles constant (carboxylate groups, negatively charged) while using two different surface modifications of AuNPs - CTAB (positively charged) and citrate (negatively charged) group modifications.

We examined the self-assembled monolayers after light irradiation of at least 10 min. We found that a closely packed ordered structure (average hexatic order $\overline{\psi_6}$ = 0.56 and average bond length $\overline{D}_B$ = 2.2 μm) forms in the "CTAB AuNP + 2 μm

https://doi.org/10.1021/acs.jpcb.4c02301
J. Phys. Chem. B 2024, 128, 9244−9254

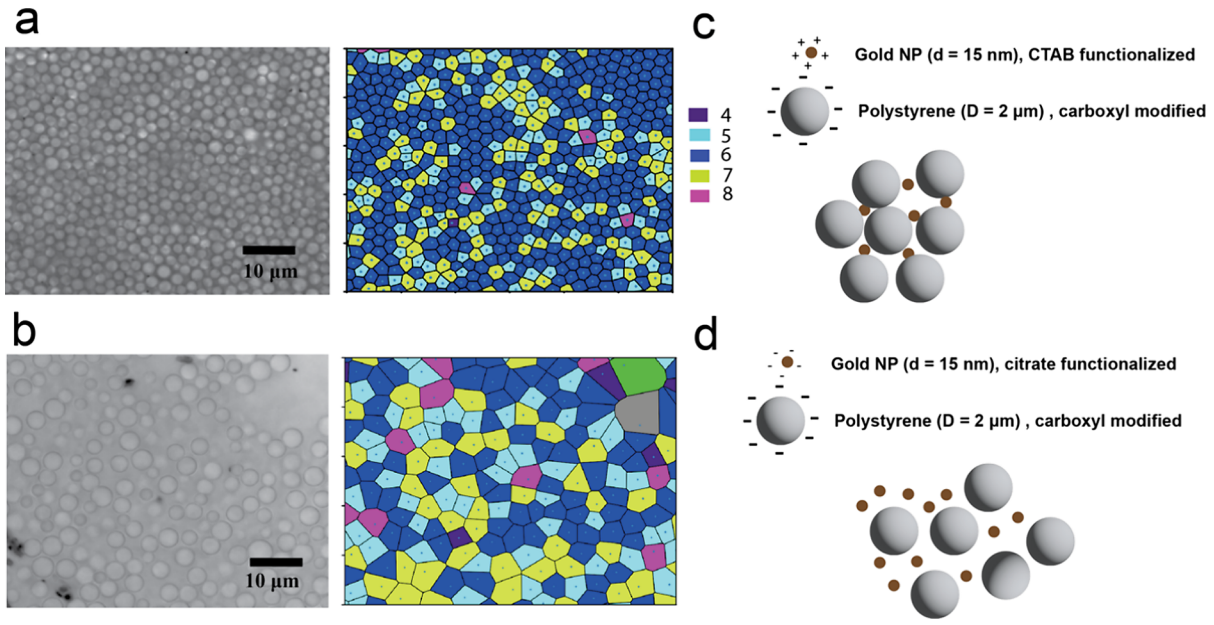

Figure 5. Effect of electrostatic interactions in photothermal self-assembly. (a) 2 μm PS particles assemble into a close-packed structure in the presence of CTAB-functionalized AuNPs. (b) 2 μm PS particles form a crowded fluid layer when mixed with citrate-functionalized AuNPs. (c) Illustration of negatively charged PS particles forming close-packed structures through the electrostatic attraction with positively charged AuNPs. (d) Illustration of negatively charged PS particles remaining in a fluid state when mixed with negatively charged AuNPs.

PS" system, as shown in Figure 5a. However, the PS particles remain in a crowded but fluid state in the "citrate AuNP + 2 μm PS" system ($\overline{\psi_6}$ = 0.36 and $\overline{D}_B$ = 4.1 μm, Figure 5b). The difference in crystalline order in between these two systems are evident from the corresponding Voronoi diagrams presented in Figure 5a,b (right). The favorable crystallization in the CTAB AuNP mixture can be explained by the electrostatic attraction between the two particle species. The positively charged CTAB groups on the gold nanoparticles help make a "bridge" between the negatively charged PS particles (illustrated in Figure 5c) that can facilitate the self-assembly of large crystalline structures. We observed the formation of small clusters (Figure S7) of PS particles in this mixture even before light illumination, indicating that electrostatic binding is present in the system. Under light irradiation, the electrostatic attraction supplements the hydrodynamic attractive attraction between particles, resulting in the formation of the close-packed assembly. We examined the reversibility of the assembly; when the light is turned off, the monolayer loses its close-packed crystalline structure but remains in a dense fluid state along with the small clusters (Figure S5). In contrast, because the "citrate AuNP + 2 μm PS" has electrostatic repulsion between the AuNPs and PS particles, the hydrodynamic interaction potential is likely not strong enough to form close-packed structures, causing the formation of a crowded fluid state. A similar nanoparticle-haloing mechanism has been reported in binary mixtures previously where highly charged nanoparticles provided colloidal stability to negligibly charged microparticles.[53] Furthermore, we found that crystallization can be induced in the "citrate AuNP + 2 μm PS" mixture by screening the repulsive Coulomb potential with an addition of 2.5 mM NaCl (Figure S6).

Next, we studied how the electrostatic interactions affect the self-assembly in binary systems of differently sized PS particles. Four additional binary systems were examined using PS particles (D = 1 and 5 μm – both negatively charged carboxylate groups) mixed with different AuNP functionalization (CTAB and citrate). We kept the AuNP size constant in all cases (d = 15 nm). Interestingly, we observe distinct colloidal phases for different PS particle size and AuNP surface functionalization. We found that there was no significant difference in crystalline order when we mixed larger sized particles (D = 5 μm) with CTAB gold NPs ($\overline{\psi_6}$ = 0.64, $\overline{D}_B$ = 5.3 μm) and citrate gold NPs ($\overline{\psi_6}$ = 0.64, $\overline{D}_B$ = 5.5 μm). In both cases, close-packed structures were observed with a high hexatic order. In contrast, the smaller PS particles with D = 1 μm did not form crystals when mixed with either CTAB or citrate-functionalized AuNPs. Instead, We found the coexistence of colloidal gels and 2D glass formation in the "CTAB AuNP + 1 μm PS" system, while particles remained in a crowded fluid state ($\overline{\psi_6}$ = 0.36, $\overline{D}_B$ = 2.2 μm) in the "citrate AuNP + 1 μm PS". As summarized in Figure 6, with decreasing

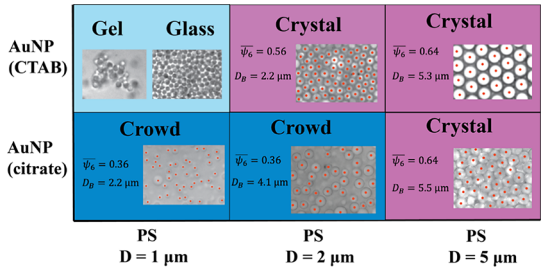

Figure 6. Summary of all phases observed in six different binary systems with varying PS particle sizes and AuNP surface functionalization.

size of PS particles, we observe a transition from crystal to crowd in the absence of electrostatic attraction, but a transition from crystal to gel in the presence of electrostatic attraction.

We explain the mechanisms of how the diverse colloidal phases emerge by carefully considering the contributions from hydrodynamic and electrostatic interactions. When particles are thermally driven to a solid surface, there is an attraction between the particles parallel to the surface due to hydrodynamics source doublet. Previous work by Leonardo et al. derived a

https://doi.org/10.1021/acs.jpcb.4c02301
J. Phys. Chem. B 2024, 128, 9244−9254

pseudopotential to account for such hydrodynamically induced attraction[44]:

$$V(r) = -V_0 \frac{a^3}{3(r^2 + 4h^2)^{3/2}} + V_0 \frac{a^5}{(r^2 + 4h^2)^{5/2}} \quad (4)$$

where, $a = \frac{D}{2}$ is the particle radius, $h \sim a$, $V_0 \propto 18\lambda a S_T \nabla T k_B T$, and λ is the Stokes correction factor. This relationship indicates that the strength and the range of the hydrodynamic interaction increase with particle size.

Using this hydrodynamic pseudopotential, we performed Monte Carlo simulations to explain how hydrodynamic interactions impact the crystallization of particles with different sizes. We estimated the temperature gradient, ∇T, from experimentally measured temperature rise and the height of the sample chamber. The Soret coefficient, S_T, is about 10 K^{-1} for micrometer-sized colloidal particles and scales quadratically with the particle size ($S_T \propto a^2$).[54] The correction factor, λ can vary by an order of magnitude within a small range of h − the distance between the center of the assembled particle layer and the solid surface,[55] indicating that the hydrodynamic attraction between particles is highly sensitive to h. We performed simulations with different values of $\frac{h}{a}$ and identified the minimum size of the particles for which the hydrodynamic interactions are strong enough to cause crystallization.

The simulations show that the onset of crystallization occurs at $a \approx 3$ μm for $h = 1.13-1.54$ a, and at $a \approx 4$ μm for $h = 2.35$ a (Figure 7a). Crystals form when the hydrodynamic attraction overrides thermal fluctuation ($18\lambda a S_T \nabla T \gg 1$), which manifests in the sudden increase in the hexatic order parameter as shown in Figure 7a. The simulation results support our experimental observations where we find crystal formation for particles with a diameter equal to or larger than $D = 5$ μm ($a = 2.5$ μm). The value of $h = 1.54$ a is also a reasonable estimate since we observe that the monolayer forms very close to the bottom wall of the sample chamber. Therefore, we can conclude that in the absence of attractive electrostatic interactions, the phase behavior observed in the "Citrate AuNP+ negatively charged PS" system can be explained by considering the hydrodynamic interactions between particles. $D = 1$ μm and $D = 2$ μm particles only form a crowded layer thanks to the convection flow (full field-of-view images in Figure S8), while a close-packed crystal forms when a strong hydrodynamic interaction potential is present, as observed in the case of $D = 5$ μm particles.

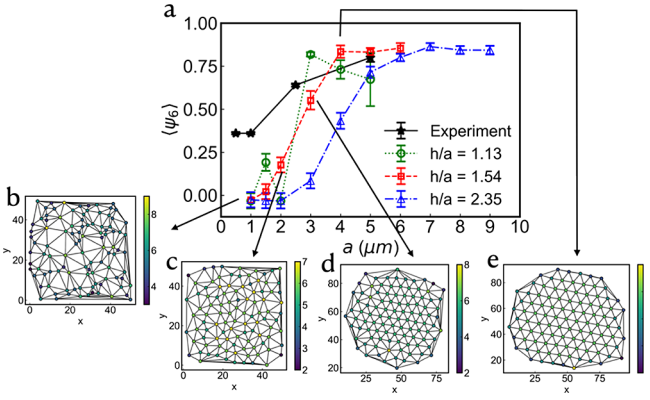

Figure 7. (a) Hexatic order parameter as a function of particle radius, a, for different vertical distances between the center of the particles in the assembled layer and the solid surface, h. Snapshots of the assemblies for (b) $a = 1$ μm, (c) $a = 2$ μm, (d) $a = 3$ μm, and (e) $a = 4$ μm (when $\frac{h}{a} = 1.54$ is used). Hexatic order parameter from the experiments (black stars) increases with a, consistent with the prediction from the simulations (all other markers). Simulation results for $h/a = 1.54$ (red squares) agree well with the experimental measurements for $a \geq 2.5$ μm. For smaller particles ($a \leq 1$ μm), the experimental order parameter is high possibly because of the flow-induced crowding that has not been considered in the simulation.

Next, we explain the rich phase behavior in the "CTAB AuNP + negatively charged PS" system where the formation of crystals and gels is observed for smaller particles ($D \leq 2$ μm) in the presence of electrostatic attraction; we can attribute these phases to favorable self-assembly kinetics. To rule out the possibility that the electrostatic interaction potential between the PS and the AuNPs could be different, we compared the surface charge density and maximum possible surface coverage of the PS particles for the three binary systems (Table 1). We find that the number of carboxyl groups and the number of AuNPs available per unit surface area of the PS particles remain almost constant for all three systems. These quantities increase marginally for larger PS particles; however, we do not observe gel formation for larger particles ($D = 2, 5$ μm) which is usually caused by strong attractive interactions. Therefore, it is likely that the kinetics of self-assembly is the major contributing factor behind the structural tunability in our experiment. For the large-sized PS particles (Diffusion constant of 0.09 $\mu m^2/s$ for $D = 5$ μm particles), it would take a long time for two particles to form bonds via oppositely charged AuNPs (as illustrated in Figure 5c). Since the photothermal assembly driven by hydrodynamic interactions occurs at a much faster time scale than diffusion (in less than a minute for $D = 5$ μm particles, Movie S2), the particles form crystals before they could form gels via diffusion. On the other hand, the much smaller PS particles ($D = 1$ μm, diffusion constant 0.5 $\mu m^2/s$) assemble into colloidal gels readily in the presence of AuNPs even before the irradiation of light (Figure S9). With light illumination, we observe a coexistence of a gel and a 2D glass phase under the combined actions of hydrodynamic and electrostatic interactions. The PS particles with middle-ranged kinetics ($D = 2$ μm, diffusion constant 0.22 $\mu m^2/s$) is a rather intriguing case where we find small clusters form (Figure S7) without light that eventually transform into a 2D crystalline layer under photothermal convection.

Table 1. Calculated Properties of Different Binary Systems

	number of carboxyl groups per unit surface area (μm^2)	number of AuNPs available per unit surface area (μm^2) of PS particles (calculated from the number ratio and the diameters of the AuNPs and PS particles)
PS ($D = 1$ μm)	1.15×10^6	5.94×10^2
PS ($D = 2$ μm)	1.35×10^6	1.43×10^3
PS ($D = 5$ μm)	8.66×10^6	3.30×10^3

CONCLUSIONS

We demonstrated that out-of-equilibrium self-assembly of colloidal particles with programmable size and tunable structural order can be achieved by photothermal mechanisms driven by gold nanoparticles. Although natural convection and thermophoresis are known for driving colloidal crystallization, the novelty of our work involves the use of a binary mixture and

https://doi.org/10.1021/acs.jpcb.4c02301
J. Phys. Chem. B 2024, 128, 9244−9254

spatial illumination control that allows for the two different kinds of tunability. Self-assembly with programmable sizes is highly relevant in the field of self-limiting assembly, where a self-assembled structure defines its finite size in equilibrium via mechanisms of geometric frustration[56,57] or self-closure.[58] Because the assembly of smaller particles ($D < 5$ μm) is reversible, the size and the shape of the particle crowd or crystal can potentially be reconfigured on demand by using different light patterns. Such shape-reconfigurable assembly provides opportunities for realizing 2-dimensional colloidal scale robots that have only been proposed in theoretical studies.[59,60] Furthermore, our work is the first to carefully examine the effect of particle size on self-assembly driven by photothermal processes, and demonstrates that strong interparticle hydrodynamic potential favors the assembly of larger particles ($D \geq 5$ μm) over smaller ones. However, electrostatic attractions between oppositely charged building block particles and gold nanoparticles can be utilized to realize diverse colloidal phases—crystallization ($D = 2$ μm), gelation ($D \leq 1$ μm), and crowd formation ($D = 1$ μm and $D = 2$ μm). The structural tunability makes our system comparable to depletion-driven self-assembly in equilibrium, where an increase in the depletant concentration and size gives rise to a transition from colloidal crystals to gels. However, the advantage of our system over any equilibrium system is the much faster time scale required for self-organization, ranging from a few seconds for $D = 2$ μm particles to a few minutes for $D = 10$ μm particles. Therefore, we conclude that the photothermal mechanisms in a binary mixture of colloidal particles truly enable the realization of rich phase behavior and shape-programmability in a relatively simple system—providing a significant leap forward in the field of light-driven, nonequilibrium self-assembly.

■ ASSOCIATED CONTENT

Supporting Information

The Supporting Information is available free of charge at https://pubs.acs.org/doi/10.1021/acs.jpcb.4c02301.

UV—vis characterization of gold nanoparticles, parameters used for temperature calculation, data on CTAB melting experiment and crowd size estimation, and supporting evidence for self-assembly mechanism (PDF)

Experimental observation showing the accumulation of gold nanoparticle clusters toward light (AVI)

Real-time observation of colloidal crystal formation in a binary mixture of polystyrene particles ($D = 5$ μm) and gold nanoparticles (AVI)

■ AUTHOR INFORMATION

Corresponding Author

Nabila Tanjeem − *Department of Physics, California State University, Fullerton, California 92831, United states;* orcid.org/0000-0002-2720-1211; Email: ntanjeem@fullerton.edu

Authors

Jose Lopez-Ceja − *Department of Mechanical Engineering, California State University, Fullerton, California 92831, United states*

Vanessa Flores − *Department of Mechanical Engineering, California State University, Fullerton, California 92831, United states*

Shirlaine Juliano − *Department of Biology, California State University, Fullerton, California 92831, United states*

Sean Machler − *Department of Physics, California State University, Fullerton, California 92831, United states*

Stephen Smith − *Department of Physics, California State University, Fullerton, California 92831, United states*

Gargi Mansingh − *Department of Physics, California State University, Fullerton, California 92831, United states*

Meng Shen − *Department of Physics, California State University, Fullerton, California 92831, United states*

Complete contact information is available at: https://pubs.acs.org/10.1021/acs.jpcb.4c02301

Notes

The authors declare no competing financial interest.

■ ACKNOWLEDGMENTS

We acknowledge financial support from the National Science Foundation (CBET, award no. 2301692) and the Office of Research and Sponsored Projects at Cal State Fullerton (RSCA award 2023—2024). We thank Dr. Wylie Ahmed and Mauricio Gomez Lopez for providing UV—vis spectroscopy support and for helpful discussions.

■ REFERENCES

(1) Hagan, M. F.; Baskaran, A. Emergent Self-Organization in Active Materials. *Curr. Opin. Cell Biol.* **2016**, *38*, 74—80.

(2) Van Ravensteijn, B. G. P.; Voets, I. K.; Kegel, W. K.; Eelkema, R. Out-of-Equilibrium Colloidal Assembly Driven by Chemical Reaction Networks. *Langmuir* **2020**, *36* (36), 10639—10656.

(3) Popescu, M. N. Chemically Active Particles: From One to Few on the Way to Many. *Langmuir* **2020**, *36* (25), 6861—6870.

(4) Palacci, J.; Sacanna, S.; Steinberg, A. P.; Pine, D. J.; Chaikin, P. M. Living Crystals of Light-Activated Colloidal Surfers. *Science* **2013**, *339* (6122), 936—940.

(5) Cates, M. E.; Tailleur, J. Motility-Induced Phase Separation. *Annual Review of Condensed Matter Physics* **2015**, *6* (1), 219—244.

(6) Zhang, J.; Alert, R.; Yan, J.; Wingreen, N. S.; Granick, S. Active Phase Separation by Turning towards Regions of Higher Density. *Nat. Phys.* **2021**, *17* (8), 961—967.

(7) Zhang, B.; Sokolov, A.; Snezhko, A. Reconfigurable Emergent Patterns in Active Chiral Fluids. *Nat. Commun.* **2020**, *11* (1), 4401.

(8) Han, K.; Kokot, G.; Tovkach, O.; Glatz, A.; Aranson, I. S.; Snezhko, A. Emergence of Self-Organized Multivortex States in Flocks of Active Rollers. *Proc. Natl. Acad. Sci. U.S.A.* **2020**, *117* (18), 9706—9711.

(9) Aubret, A.; Youssef, M.; Sacanna, S.; Palacci, J. Targeted Assembly and Synchronization of Self-Spinning Microgears. *Nat. Phys.* **2018**, *14* (11), 1114—1118.

(10) Bäuerle, T.; Löffler, R. C.; Bechinger, C. Formation of Stable and Responsive Collective States in Suspensions of Active Colloids. *Nat. Commun.* **2020**, *11* (1), 2547.

(11) Yan, J.; Han, M.; Zhang, J.; Xu, C.; Luijten, E.; Granick, S. Reconfiguring Active Particles by Electrostatic Imbalance. *Nat. Mater.* **2016**, *15* (10), 1095—1099.

(12) Martínez-Pedrero, F.; Ortega, F.; Rubio, R. G.; Calero, C. Collective Transport of Magnetic Microparticles at a Fluid Interface through Dynamic Self-Assembled Lattices. *Adv. Funct. Mater.* **2020**, *30* (50), No. 2002206.

(13) Yang, Q.; Zhu, H.; Liu, P.; Liu, R.; Shi, Q.; Chen, K.; Zheng, N.; Ye, F.; Yang, M. Topologically Protected Transport of Cargo in a Chiral Active Fluid Aided by Odd-Viscosity-Enhanced Depletion Interactions. *Phys. Rev. Lett.* **2021**, *126* (19), No. 198001.

(14) Han, K.; Shields, C. W.; Bharti, B.; Arratia, P. E.; Velev, O. D. Active Reversible Swimming of Magnetically Assembled "Microscallops" in Non-Newtonian Fluids. *Langmuir* **2020**, *36*, 7148.

(15) Dreyfus, R.; Baudry, J.; Roper, M. L.; Fermigier, M.; Stone, H. A.; Bibette, J. Microscopic Artificial Swimmers. *Nature* **2005**, *437* (7060), 862−865.
(16) Vialetto, J.; Anyfantakis, M.; Rudiuk, S.; Morel, M.; Baigl, D. Photoswitchable Dissipative Two-Dimensional Colloidal Crystals. *Angew. Chem., Int. Ed.* **2019**, *58* (27), 9145−9149.
(17) Oh, J. S.; Yi, G.-R.; Pine, D. J. Reconfigurable Transitions between One- and Two-Dimensional Structures with Bifunctional DNA-Coated Janus Colloids. *ACS Nano* **2020**, *14* (11), 15786−15792.
(18) Kuzyk, A.; Yang, Y.; Duan, X.; Stoll, S.; Govorov, A. O.; Sugiyama, H.; Endo, M.; Liu, N. A Light-Driven Three-Dimensional Plasmonic Nanosystem That Translates Molecular Motion into Reversible Chiroptical Function. *Nat. Commun.* **2016**, *7*, 10591.
(19) Bharti, B.; Velev, O. D. Assembly of Reconfigurable Colloidal Structures by Multidirectional Field-Induced Interactions. *Langmuir* **2015**, *31* (29), 7897−7908.
(20) Lee, J.; Ku, K. H.; Park, C. H.; Lee, Y. J.; Yun, H.; Kim, B. J. Shape and Color Switchable Block Copolymer Particles by Temperature and pH Dual Responses. *ACS Nano* **2019**, *13* (4), 4230−4237.
(21) Kim, J.; Choi, S.-E.; Lee, H.; Kwon, S. Magnetochromatic Microactuators for a Micropixellated Color-Changing Surface. *Adv. Mater.* **2013**, *25* (10), 1415−1419.
(22) Lim, S.; Song, J. E.; La, J. A.; Cho, E. C. Gold Nanospheres Assembled on Hydrogel Colloids Display a Wide Range of Thermoreversible Changes in Optical Bandwidth for Various Plasmonic-Based Color Switches. *Chem. Mater.* **2014**, *26* (10), 3272−3279.
(23) Chen, X.; Lin, L.; Li, Z.; Sun, H.-B. Light-Directed Assembly of Colloidal Matter. *Adv. Funct. Mater.* **2022**, *32* (22), No. 2104649.
(24) Kim, Y.; Shah, A. A.; Solomon, M. J. Spatially and Temporally Reconfigurable Assembly of Colloidal Crystals. *Nat. Commun.* **2014**, *5* (1), 3676.
(25) Hayward, R. C.; Saville, D. A.; Aksay, I. A. Electrophoretic Assembly of Colloidal Crystals with Optically Tunable Micropatterns. *Nature* **2000**, *404* (6773), 56−59.
(26) Palacci, J.; Sacanna, S.; Kim, S.-H.; Yi, G.-R.; Pine, D. J.; Chaikin, P. M. Light-Activated Self-Propelled Colloids. *Philos. Trans. R. Soc., A* **2014**, *372* (2029), 20130372.
(27) Singh, D. P.; Choudhury, U.; Fischer, P.; Mark, A. G. Non-Equilibrium Assembly of Light-Activated Colloidal Mixtures. *Adv. Mater.* **2017**, *29* (32), No. 1701328.
(28) Arya, P.; Feldmann, D.; Kopyshev, A.; Lomadze, N.; Santer, S. Light Driven Guided and Self-Organized Motion of Mesoporous Colloidal Particles. *Soft Matter* **2020**, *16* (5), 1148−1155.
(29) Vutukuri, H. R.; Lisicki, M.; Lauga, E.; Vermant, J. Light-Switchable Propulsion of Active Particles with Reversible Interactions. *Nat. Commun.* **2020**, *11* (1), 2628.
(30) Ben Zion, M. Y.; Caba, Y.; Modin, A.; Chaikin, P. M. Cooperation in a Fluid Swarm of Fuel-Free Micro-Swimmers. *Nat. Commun.* **2022**, *13* (1), 184.
(31) Chen, Z.; Li, J.; Zheng, Y. Heat-Mediated Optical Manipulation. *Chem. Rev.* **2022**, *122* (3), 3122−3179.
(32) Chen, H.; Gratton, E.; Digman, M. A. Self-Assisted Optothermal Trapping of Gold Nanorods under Two-Photon Excitation. *Methods Appl. Fluoresc.* **2016**, *4* (3), No. 035003.
(33) Flores-Flores, E.; Torres-Hurtado, S. A.; Páez, R.; Ruiz, U.; Beltrán-Pérez, G.; Neale, S. L.; Ramirez-San-Juan, J. C.; Ramos-García, R. Trapping and Manipulation of Microparticles Using Laser-Induced Convection Currents and Photophoresis. *Biomed. Opt. Express, BOE* **2015**, *6* (10), 4079−4087.
(34) Kang, Z.; Chen, J.; Wu, S.-Y.; Chen, K.; Kong, S.-K.; Yong, K.-T.; Ho, H.-P. Trapping and Assembling of Particles and Live Cells on Large-Scale Random Gold Nano-Island Substrates. *Sci. Rep* **2015**, *5* (1), 9978.
(35) Kang, Z.; Chen, J.; Wu, S.-Y.; Ho, H.-P. Plasmonic Absorption Activated Trapping and Assembling of Colloidal Crystals with Non-Resonant Continuous Gold Films. *RSC Adv.* **2015**, *5*, 105409−105415.
(36) Park, J.; Lee, S.; Lee, H.; Han, S.; Kang, T. H.; Kim, D.; Kang, T.; Choi, I. Colloidal Multiscale Assembly via Photothermally Driven Convective Flow for Sensitive In-Solution Plasmonic Detections. *Small* **2022**, *18* (24), No. 2201075.
(37) Dinh, N.-D.; Luo, R.; Christine, M. T. A.; Lin, W. N.; Shih, W.-C.; Goh, J. C.-H.; Chen, C.-H. Effective Light Directed Assembly of Building Blocks with Microscale Control. *Small* **2017**, *13* (24), No. 1700684.
(38) Brasiliense, V.; Berto, P.; Aubertin, P.; Maisonhaute, E.; Combellas, C.; Tessier, G.; Courty, A.; Kanoufi, F. Light Driven Design of Dynamical Thermosensitive Plasmonic Superstructures: A Bottom-Up Approach Using Silver Supercrystals. *ACS Nano* **2018**, *12* (11), 10833−10842.
(39) Sharma, V.; Paul, D.; Chaubey, S. K.; Tiwari, S.; Kumar, G. V. P. Large-Scale Optothermal Assembly of Colloids Mediated by a Gold Microplate. *J. Phys.: Condens. Matter* **2020**, *32* (32), 324002.
(40) Lin, L.; Zhang, J.; Peng, X.; Wu, Z.; Coughlan, A. C. H.; Mao, Z.; Bevan, M. A.; Zheng, Y. Opto-Thermophoretic Assembly of Colloidal Matter. *Science Advances* **2017**, *3* (9), No. e1700458.
(41) Jin, C. M.; Lee, W.; Kim, D.; Kang, T.; Choi, I. Photothermal Convection Lithography for Rapid and Direct Assembly of Colloidal Plasmonic Nanoparticles on Generic Substrates. *Small* **2018**, *14* (45), No. 1803055.
(42) Liu, Z.; Lei, J.; Zhang, Y.; Tang, X.; Zhang, Y.; Zhao, E.; Yang, J.; Yuan, L. Light-Induced Thermal Convection for Size-Based Microparticle Sorting. *J. Opt. Soc. Am. B, JOSAB* **2016**, *33* (9), 1881−1887.
(43) Duhr, S.; Braun, D. Two-Dimensional Colloidal Crystals Formed by Thermophoresis and Convection. *Appl. Phys. Lett.* **2005**, *86* (13), 131921.
(44) Di Leonardo, R.; Ianni, F.; Ruocco, G. Colloidal Attraction Induced by a Temperature Gradient. *Langmuir* **2009**, *25* (8), 4247−4250.
(45) Garcés-Chávez, V.; Quidant, R.; Reece, P. J.; Badenes, G.; Torner, L.; Dholakia, K. Extended Organization of Colloidal Microparticles by Surface Plasmon Polariton Excitation. *Phys. Rev. B* **2006**, *73* (8), No. 085417.
(46) Ramírez-Ramírez, J.; Sarabia-Alonso, J. A.; Vázquez-Lozano, J.; Peregrina-Barreto, H.; Mansurova, S.; Ramos-García, R. Formation and Manipulation of 2D Colloidal Crystals Driven by Convective Currents and Electrostatic Forces. *Optics & Laser Technology* **2023**, *161*, No. 109117.
(47) Nikoobakht, B.; El-Sayed, M. A. Preparation and Growth Mechanism of Gold Nanorods (NRs) Using Seed-Mediated Growth Method. *Chem. Mater.* **2003**, *15* (10), 1957−1962.
(48) Liu, X.; Wei, R.; Hoang, P. T.; Wang, X.; Liu, T.; Keller, P. Reversible and Rapid Laser Actuation of Liquid Crystalline Elastomer Micropillars with Inclusion of Gold Nanoparticles. *Adv. Funct. Mater.* **2015**, *25* (20), 3022−3032.
(49) Rivière, D.; Selva, B.; Chraibi, H.; Delabre, U.; Delville, J.-P. Convection Flows Driven by Laser Heating of a Liquid Layer. *Phys. Rev. E* **2016**, *93* (2), No. 023112.
(50) Govorov, A. O.; Richardson, H. H. Generating Heat with Metal Nanoparticles. *Nano Today* **2007**, *2* (1), 30−38.
(51) Govorov, A. O.; Zhang, W.; Skeini, T.; Richardson, H.; Lee, J.; Kotov, N. A. Gold Nanoparticle Ensembles as Heaters and Actuators: Melting and Collective Plasmon Resonances. *Nanoscale Res. Lett.* **2006**, *1* (1), 84.
(52) Weinert, F. M.; Braun, D. Observation of Slip Flow in Thermophoresis. *Phys. Rev. Lett.* **2008**, *101* (16), No. 168301.
(53) Tohver, V.; Smay, J. E.; Braem, A.; Braun, P. V.; Lewis, J. A. Nanoparticle Halos: A New Colloid Stabilization Mechanism. *Proc. Natl. Acad. Sci. U. S. A.* **2001**, *98* (16), 8950−8954.
(54) Duhr, S.; Braun, D. Why Molecules Move along a Temperature Gradient. *Proc. Natl. Acad. Sci. U. S. A.* **2006**, *103* (52), 19678−19682.
(55) Happel, J.; Brenner, H. *Low Reynolds Number Hydrodynamics: With Special Applications to Particulate Media*; Moreau, R. J., Series Ed.; Mechanics of fluids and transport processes; Springer Netherlands: Dordrecht, 1983; Vol. *1*.
(56) Hagan, M. F.; Grason, G. M. Equilibrium Mechanisms of Self-Limiting Assembly. *Rev. Mod. Phys.* **2021**, *93* (2), No. 025008.

(57) Tanjeem, N.; Hall, D. M.; Minnis, M. B.; Hayward, R. C.; Grason, G. M. Focusing Frustration for Self-Limiting Assembly of Flexible, Curved Particles. *Phys. Rev. Research* **2022**, *4* (3), No. 033035.
(58) Hayakawa, D.; Videbaek, T. E.; Hall, D. M.; Fang, H.; Sigl, C.; Feigl, E.; Dietz, H.; Fraden, S.; Hagan, M. F.; Grason, G. M.; et al. Geometrically Programmed Self-Limited Assembly of Tubules Using DNA Origami Colloids. *Proc. Natl. Acad. Sci. U. S. A.* **2022**, *119* (43), No. e2207902119.
(59) VanSaders, B.; Glotzer, S. C. Sculpting Crystals One Burgers Vector at a Time: Toward Colloidal Lattice Robot Swarms. *Proc. Natl. Acad. Sci. U. S. A.* **2021**, *118* (3), No. e2017377118.
(60) Agrawal, M.; Glotzer, S. C. Scale-Free, Programmable Design of Morphable Chain Loops of Kilobots and Colloidal Motors. *Proc. Natl. Acad. Sci. U.S.A.* **2020**, *117* (16), 8700−8710.

https://doi.org/10.1021/acs.jpcb.4c02301
J. Phys. Chem. B 2024, 128, 9244−9254